Article

Transverse Electromagnetic Mode Conversion for High-Harmonic Self-Probing Spectroscopy

Antoine Camper [1], Amélie Ferré [2], Nan Lin [1], Emmanouil Skantzakis [1], David Staedter [3], Elizabeth English [1], Bastian Manschwetus [1,†], Frédéric Burgy [2], Stéphane Petit [2], Dominique Descamps [2], Thierry Auguste [1], Olivier Gobert [1], Bertrand Carré [1], Pascal Salières [1], Yann Mairesse [2] and Thierry Ruchon [1,*]

[1] CEA, IRAMIS, Lasers, Interactions and Dynamics Laboratory - LIDyL, CEA-Saclay, F-91191 Gif-sur-Yvette, France; E-Mail: antoine.camper@cea.fr (A.C.); linnan711@gmail.com (N.L.); skanman@iesl.forth.gr (E.S.); ee.laser@gmail.com (E.E.); bastian.manschwetus@gmail.com (B.M.); thierry.auguste@cea.fr (T.A.); olivier.gobert@cea.fr (O.G.); bertrand.carre@cea.fr (B.C.); pascal.salieres@cea.fr (P.S.)

[2] Université de Bordeaux - CNRS - CEA, CELIA, UMR5107, F33405 Talence, France; E-Mail: amelie_ferre@orange.fr (A.F.); burgy@celia.u-bordeaux1.fr (F.B.); petit@celia.u-bordeaux1.fr (S.P.); descamps@celia.u-bordeaux1.fr (D.D.); mairesse@celia.u-bordeaux1.fr (Y.M.)

[3] Université de Toulouse - CNRS, LCAR-IRSAMC, 31062 Toulouse Cedex 09, France; E-Mail: dstaedter@gmail.com

[†] Current address: Department of Physics Atomic Physics Lund University Box 118, SE-221-00 Lund, Sweden

[*] Author to whom correspondence should be addressed; E-Mail: thierry.ruchon@cea.fr; Tel.: +331-690-87-010/+331-690-88-707.

Abstract: We report on high-order harmonic (HHG) two-source interferometry (TSI) in molecular gases. We used a 0-π phase plate to create two bright spots at the focus of a lens by converting a Gaussian laser beam into a TEM_{01} Transverse Electromagnetic Mode. The two bright foci produce two synchronized HHG sources. One of them is used to probe on-going dynamics in the generating medium, while the other serves to heterodyne the signal. We first compute overlap integrals to investigate the mode conversion efficiency. We then establish a clear relation between the laser phase-front curvature and the far-field overlap of the two HHG beams. Both Fresnel diffraction calculations and an experimental lens position scan

are used to reveal variations of the phase front inclination in each source. We show that this arrangement offers $\frac{\lambda_{XUV}}{100}$ precision, enabling extremely sensitive phase measurements. Finally, we use this compact setup for TSI and measure phase variations across the molecular alignment revival of nitrogen and in vibrating sulfur hexafluoride. In both gases, the phase variations change sign around the ionization threshold of the investigated molecule.

Keywords: HHG; two-source interferometry; XUV; diffractive optical element; attosecond

PACS classifications: 32.70.-n, 42.65.Ky, 42.65.Re

---

1. Introduction

Self-probing spectroscopy based on high-order harmonic generation (HHG) has proven to greatly benefit from phase measurements, both for structural and dynamic studies of the generating medium [1–3]. Indeed, the infrared (IR) laser-driven electron rescattering process [4–6] leading to the emission of harmonic combs in the extreme ultra-violet (XUV) allows one to probe atoms and molecules *in situ* with unprecedented attosecond time resolution and Ångström precision. In particular, the phase of the attosecond emission gives access to photo-recombination Wigner delays [2,7,8] and phase difference in multi-channel ionization of aligned molecules [3,9]. Specific techniques have been developed to measure phases in the XUV domain [1,3,10–13] and unravel this subtle information. All of these interferometric techniques require the synchronization of two light or matter waves (the one to be characterized and a reference) with sub-femtosecond precision. In HHG two-source interferometry (TSI), the two light waves are overlapped in the far-field to form fringes on a phosphor screen (see Figure 1). The position on the screen of the latter one directly reflects the phase difference between the two emissions. In a recent paper [14], we reported the use of a 0-π phase plate to convert a Gaussian beam into a TEM_{01} Transverse Electromagnetic Mode and created two bright spots at the focus of a lens. These two foci were used as two spatially separated and synchronized HHG sources. We qualified this setup for TSI self-probing spectroscopy with full three-dimensional simulations of the generation process and experimental phase measurements in aligned carbon dioxide. Here, we give a more thorough insight into this 0-π phase plate interferometer, how it works, its precision and its stability. The spatial interferogram analysis procedure is also described. We then report the phase measurements using this setup and demonstrate that subtle information about nitrogen alignment revivals and sulfur hexafluoride Raman vibrations can be followed through harmonics phase variations. These results reveal phase variations with opposite behaviors below and above a threshold. This method could be used to assign HHG to one specific ionization channel in molecules having several orbitals contributing to the non-linear process.
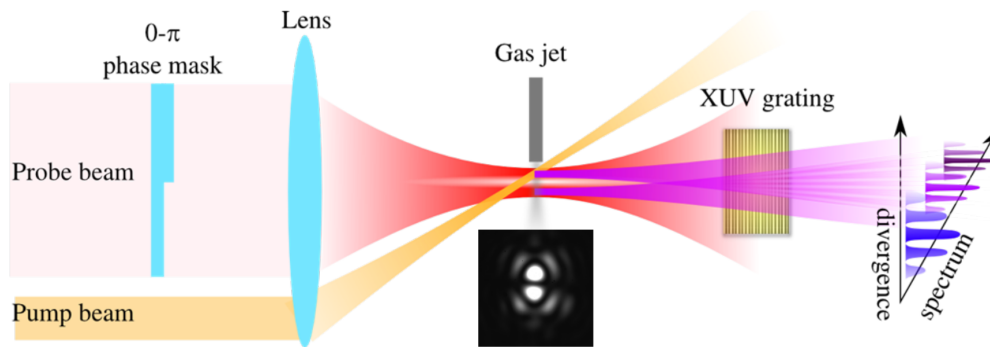
Figure 1. (Color on-line) A 0-π phase plate is used as a mode convertor for HHG phase measurement by twp-source interferometry (TSI). The inset below the gas jet shows an experimental picture of the two bright spots created at the focus of a lens with a 0-π phase plate on the LUCAlaser. One of the two sources is used as a probe of the dynamics induced by a pump beam that is overlapped only with this source. The other HHG source remains unexcited and is used as a reference. A set of micro-channel plates and a phosphor screen are placed in the flat-field of a variable groove grating that allows one to disperse the different harmonic orders in one dimension and resolve their spatial profile in the other dimension. The overlap of the two emissions in the far-field results in interference fringes. Their position directly reflects the phase difference between the two HHG sources.

2. Phase-Plate Mode Conversion

Interferometric precision is more and more demanding as the central frequency of the signal increases. In particular, interferograms in the XUV-domain [15] require highly stable experimental arrangements (for instance, the wavelength of H_{21}, the 21st harmonic order of a 800-nm laser, is about 38 nm). In TSI, the reference beam is used to heterodyne the signal, *id est*, the signal is transferred to a lower frequency. Recently, several TSI schemes were developed using amplitude division [15–18] and wave-front division [1,19]. All-transmissive schemes are more adapted to this kind of experiment than a Michelson or Mach–Zehnder interferometer, since they intrinsically offer higher stability. In a recent paper [20], TSI was implemented to determine the amount of orbital angular momentum carried by HHG using diffractive optical element (DOE) beam splitting [21]. In [14], we instead based our two source setup on the spatial mode conversion of the driving laser beam. In the absence of a chirp-pulse amplification (CPA) digital laser [22] providing on-demand mode femtosecond pulses, we used a 0-π phase plate to implement the mode conversion [23–26]. As shown in Figure 2a, we computed the overlap integral between the Gaussian phase-plate-shaped beam (GSB; see Figure 2c) of waist ω_0 and a TEM_{01} mode. Both electric fields are considered collimated. We find that a maximum of 90.94% of the input Gaussian beam is converted into the TEM_{01} mode of waist $\omega = 0.58 \times \omega_0$. This value is slightly smaller than the 93% reported in [26], but still rather close. This conversion rate could be improved by using a cylindrical lens to adjust the waist of the transmitted beam in the direction orthogonal to the 0-π step. In Figure 2b, we show the overlap integral between the GSB and higher TEM_{0i} modes with waist $\omega = 0.58 \times \omega_0$. As expected, the overlap integral with TEM_{02i} modes is zero, while TEM_{04j+1} and TEM_{04j+3} contribute with opposite signs and a decreasing amplitude as j increases. These higher order

contributions are revealed at the focus of a lens as diffraction peaks in the surroundings of the two bright spots of interest. However, the intensity in these undesired diffraction patterns is not strong enough to induce the HHG non-linear non-perturbative process (see [14]).
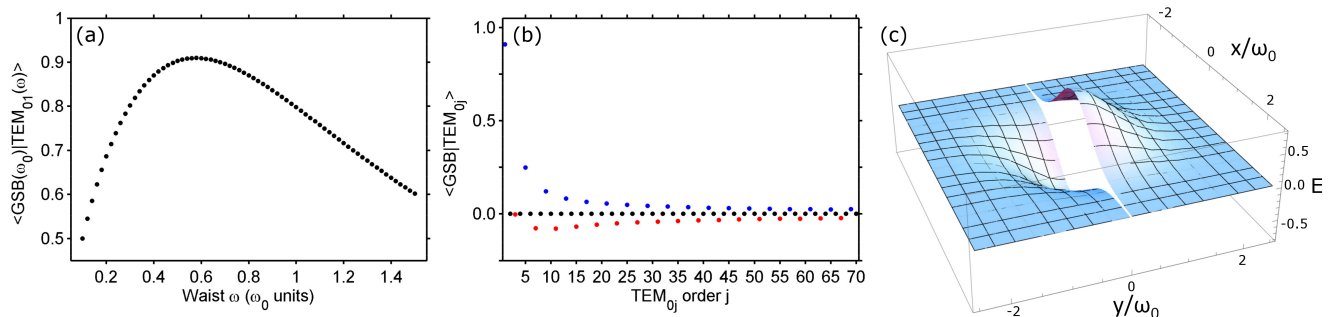

Figure 2. (Color on-line) (**a**) Conversion efficiency from a TEM_{00} mode with waist ω_0 to a TEM_{01} mode with waist ω using a 0-π phase step as a mode convertor. The conversion efficiency is computed as the overlap integral between the Gaussian phase-plate-shaped beam (GSB) and a TEM_{01} beam of waist ω. A maximum of 90.94% is reached for $\omega = 0.58 \times \omega_0$. (**b**) Decomposition of the spatial profile of the beam after the phase plate in the TEM_{0i} basis. Each coefficient is calculated as the overlap integral between the GSB and the TEM_{0i} mode of waist $0.58 \times \omega_0$. TEM_{02i} modes do not contribute. TEM_{04j+1} (blue dots) and TEM_{04j+3} (red dots) modes contribute with opposite signs. (**c**) Three–dimensional view of the GSB electric field.

As the conclusion of this section, we would like to emphasize that this spatial mode conversion approach is more efficient than the DOE beam splitting one that allows at best to focus 81.1% in the two spatially-separated bright spots. Moreover, the mode conversion approach creates the two foci in the zeroth order of diffraction, which results in a smaller source-to-source distance than the DOE beam splitting method and contributes to transferring the signal to smaller spatial frequencies. In the next section, we study the effect of the IR laser phase front curvature on the far-field overlap of the two HHG beams.

3. Far-Field Overlap

HHG in the gas phase is a macroscopic emission process and is therefore subjected to specific phase matching conditions. These conditions are strongly influenced by the phase of the microscopic harmonic dipole moment, which was shown to depend linearly on the laser intensity [27,28]. Consequently, intensity variations in the fundamental beam induce strong phase variations in the harmonic emission. By contrast, in the vicinity of a maximum, this phase is stationary, such that harmonics are emitted along the direction orthogonal to the local phase front. In each bright spot created by the phase plate at the focus of a lens, the phase front inclination at the peak intensity determines the direction in which the harmonics are emitted. If the phase front tilt in the two foci is unfavorable, the two harmonic beams may not overlap in the far-field, preventing interferences. Figure 3a shows the phase front of the GSB at the focus of a 1-m focusing lens (central column) and 10 mm upstream

(left column) and downstream (right column) of the focus. While at the exact focus position, the phase front is almost flat on both sides of the 0-π phase step, a slope appears outside of focus. In order to estimate its impact on HHG, we evaluate this slope at the position of the two harmonic sources, *id est*, at the points of maximum laser intensity. Figure 3b shows the phase front inclination for each source as a function of the distance along the propagation axis. The two sources see opposite phase slopes, so that, in general, they will emit in different directions. A positive sign in the upper (respectively lower) source phase front slope indicates that the harmonics are propagating towards (resp. away from) the optical axis. We conclude that there is only one position along the propagation direction for which the two emissions are emitted parallel to one another. Note that in this case, the harmonics from the two sources do not propagate along the IR propagation axis, but they are emitted with a small angle (the value of the slope when the two curves cross is not zero). This condition is reached when the jet is placed shortly downstream of the laser focus. This position is known for allowing the phase-matching of both short and long trajectories [27,28]. To conclude this discussion, if the gas target is far enough away from the laser focus (upstream or downstream), the harmonic emission from the two sources will no longer overlap and will not interfere. When the laser focus is placed upstream of the gas jet ($z_f < 0$), the upper (resp. lower) harmonic emission measured in the far-field will be generated by the upper (resp. lower) source, whereas it will result from the lower (resp. upper) bright spot non-linear interaction with the generating medium if the latter is placed downstream of the laser focus.
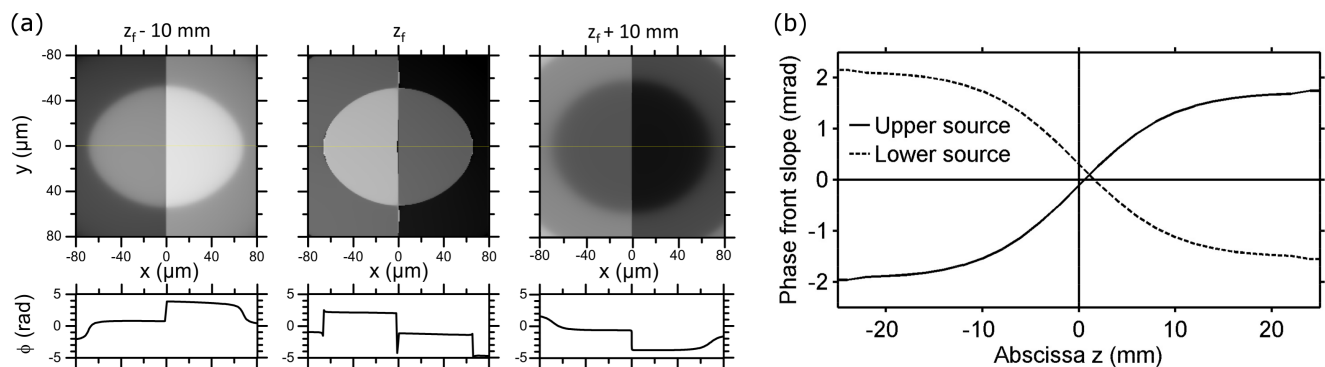

Figure 3. (**a**) Phase front bidimensional maps (first row) and lineouts along y = 0 (second row) of a Gaussian laser beam shaped with a 0-π phase plate 10 mm upstream of the focus of a 1-m lens (left) (z_f–10 mm), at the focus (center) (z_f) and 10 mm downstream of the focus (right) (z_f+10 mm). The beam diameter is 32.4 mm at $1/e^2$. It is apertured down to 15 mm and has a 10-mm hole centered on-axis. This annular beam geometry corresponds to the one used with the LUCA laser. We checked that the results presented here are still valid for the Gaussian geometry used for the Aurore laser. (**b**) Phase front inclination at peak intensity across the laser focus in, respectively, the upper (solid line) and lower (dashed line) source.

To investigate experimentally the influence of the phase front inclination, we generated harmonics using the Aurore Ti:sapphire laser system at CELIA, which delivers 8 mJ, 25-fs pulses at 1 kHz (see also the results presented in [14]). A hard aperture of 7 mm in diameter was placed in the laser beam. Harmonics were produced by focusing the phase-shaped beam in a 250 μm-thick continuous jet of nitrogen gas with a lens of 500 mm in focal length. The phosphor screen is about 500 mm away from

the two sources. Figure 4 shows the far-field spatial profile of H_9 to H_{17} as a function of the laser focus with respect to the gas jet position. These measurements confirm that the two sources generally emit harmonics in different directions. Interferences are only observed when the focus is close to the gas jet position. This condition is even more strict for higher harmonics. In addition, for H_{15} and H_{17} generated close to the focus, one can clearly identify out-of-axis contributions that can be related to long-trajectory HHG. Although this part of the emission also features fringes, the phase in the short-trajectory HHG can still be analyzed, since the two contributions are spatially separated.
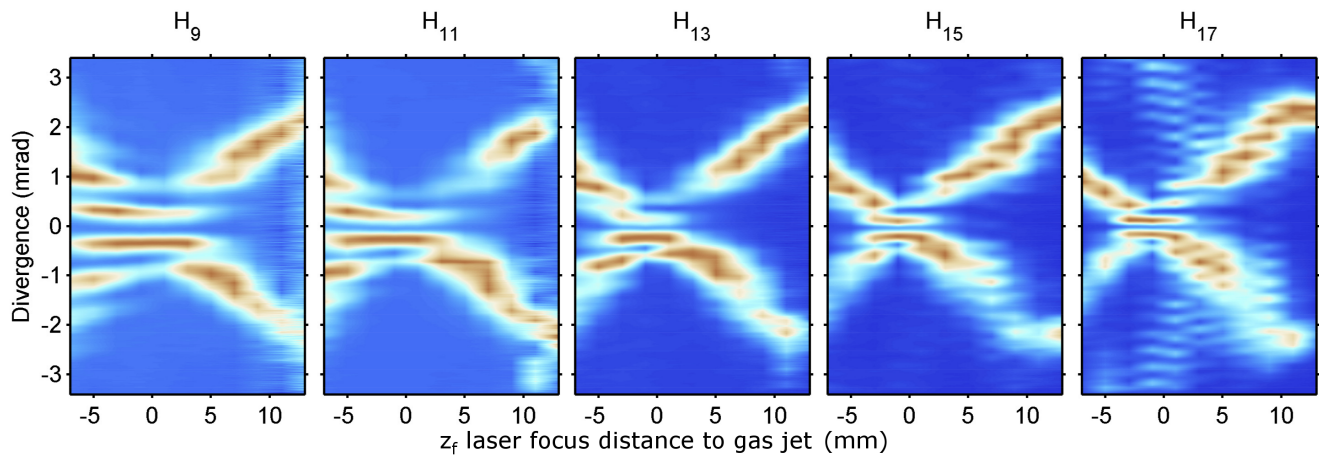

Figure 4. (Color on-line) Far-field profile of H_9 to H_{17} of the Aurore laser at CELIAgenerated with a 0-π phase-plate when the gas jet is moved through the focus. The peak intensity has been normalized for each harmonic and each position of the gas jet. The gas target is nitrogen.

After optimizing the focus position, we study the harmonic interference pattern over a broad spectral range by generating in sulfur hexafluoride (SF_6). This broad-band spectrum presented in Figure 5a results from the juxtaposition of the first and second diffraction orders of the XUV-grating. H_9 to H_{17} were obtained from the first order of diffraction and H_{19} to H_{35} from the second order. The relative amplitude between the two spectra was adjusted following the results presented in [29]. Figure 5b shows the amplitude of the one-dimensional Fourier transform of the above spectrum along the vertical dimension. The dashed line emphasizes the linear relation between the interferogram spatial frequencies and the photon energies:

$$\tilde{k}_q = q \times \frac{2\pi}{\lambda_0} \frac{a}{D} = k_q \times \Gamma \tag{1}$$

where D is the source-to-screen distance, a the distance between the two sources, $\Gamma = \frac{a}{D}$ the spatial frequency demagnification rate, λ_0 the IR fundamental wavelength, q the harmonic order and $k_q = q \times \frac{2\pi}{\lambda_0}$ the $q-th$ harmonic order wave vector modulus. The dispersion described in Equation (1) is expected from the analogy with the Young double-slit experiment. In particular, the spatial frequencies are proportional to the source spacing, and the smaller a, the higher spatial frequencies can be resolved. We believe that our mode conversion approach offers the smallest source-to-source distance possible, since in this case, a is only twice the full width at half maximum (FWHM) of one source (see [14]).
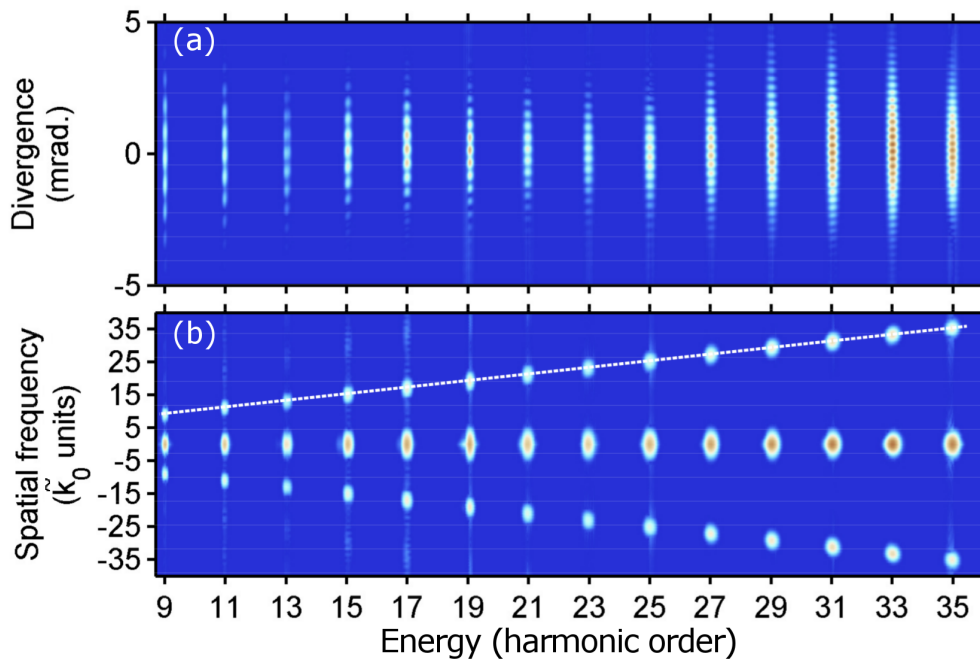
Figure 5. (Color on-line) (**a**) Interference pattern in the SF_6 HHG spectrum reconstructed from the first (H_9 to H_{17}) and second order (H_{19} to H_{35}) of diffraction of the grating; (**b**) Fourier transform decomposition in spatial frequencies of the interferogram presented in (a). The dashed line reveals the Young double-slit linear dispersion. Spatial frequencies are given in $\tilde{k}_0 = \frac{2\pi}{\lambda_0} \times \Gamma$ units (see Equation (1) in the text).

Equation (1) can also be used to gain insight into TSI bandwidth limitations imposed by its intrinsic achromatic demagnification rate Γ. At low photon energies, Γ might be too weak. At least one full period of the spatial oscillation is required to determine the phase difference between the two emissions. Considering in first approximation that all harmonic orders have the same divergence, there is a lower photon energy limit for which this condition is no longer met. At high energies, the highest spatial frequency that can be resolved by the detector following the Shannon–Nyquist criteria is finally limited to half the inverse of the center-to-center pixel distance of the CCD camera imaging the phosphor screen. The spatial spectrogram presented in Figure 5a is within these limits.

The dispersion relation of Equation (1) is also found in Figure 6, which features far-field profile lineouts (Panel a) of H_{17} to H_{29} generated in nitrogen with LUCA (100 mJ, 20 Hz, 60 fs, CPAlaser system available at CEA-Saclay) and both the phase (Panel b) and amplitude (Panel c) of the Fourier transform of these fringe patterns. The imaging system used in this experiment has a lower resolution than the one used at CELIA, and the spatial frequency in H_{29} is close to the highest that can be resolved. In the next section, we use the harmonics generated in nitrogen to investigate the precision on phase measurements and the stability of our phase-plate mode conversion interferometer.
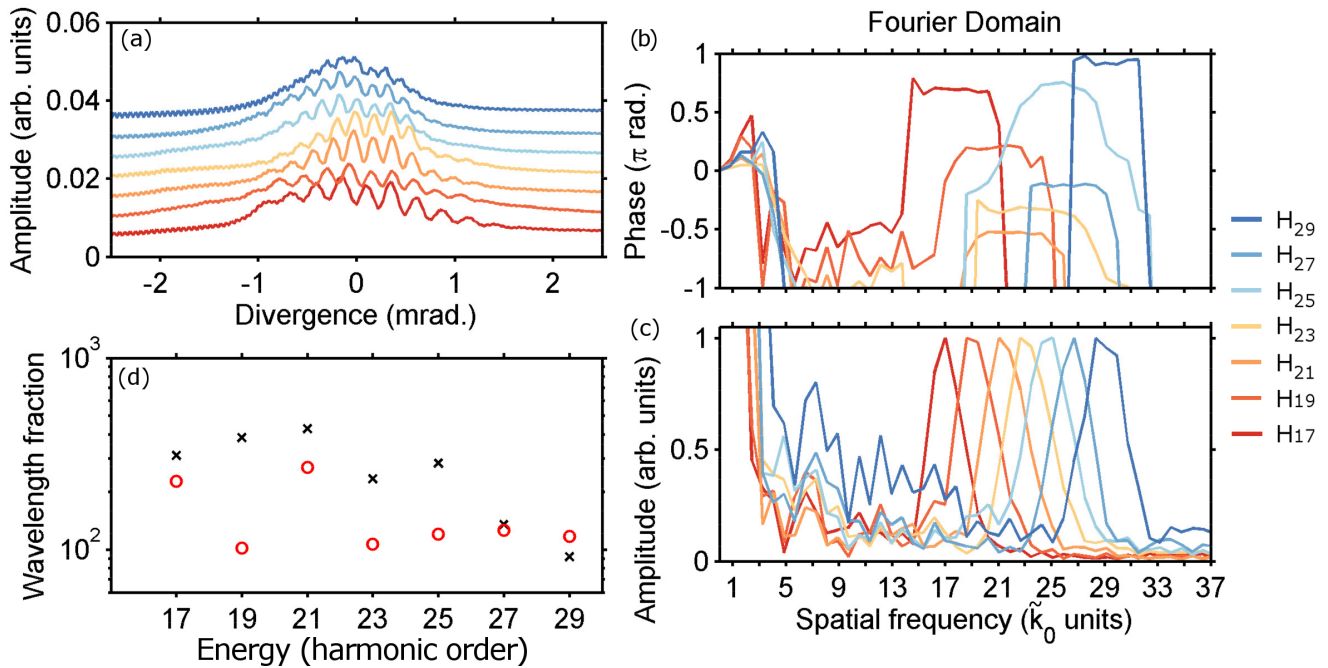
Figure 6. (Color on-line) (**a**) The fringes' lineout of H_{17} (red) to H_{29} (blue) generated in nitrogen with the LUCA laser. Each harmonic order was integrated over a 0.2-photon unit interval centered at the harmonic frequency; the harmonic spatial profiles have been arbitrarily shifted for clarity; (**b**) phase and (**c**) amplitude of the Fourier transform of each fringe pattern presented in (a); the phase has been wrapped, so that its variations around the amplitude peak are clearly visible for each harmonic order. The amplitude has been normalized at the non-zero spatial frequency peak. (**d**) The red circles represent the precision of the interferometer evaluated as 2π times the inverse of the standard deviation of the phase over the spatial frequency width of each amplitude peak. The black "x"-shaped crosses indicate the long-term stability of the interferometer estimated as 2π times the inverse of the standard deviation of the phase for about ten thousand shots.

4. Resolution and Stability of the Interferometer

To extract the phase from the interferogram, we choose to integrate each harmonic far-field profile over a fraction of the fundamental photon unit centered at the harmonic frequency and Fourier transform the result. The Fourier transform includes a circular shift of the fringe pattern to account for the linear contribution to the phase inherent to a shift of the center of mass of the harmonic profile with respect to the center of the detector. Figure 6b presents the phase of the Fourier transform of the fringe profiles presented in panel Figure 6a. This phase appears to be well-defined, since it keeps a constant value over the spatial frequency range of the associated amplitude peak (Figure 6c). The value of the HHG phase difference between the two emissions is calculated as the mean value of the Fourier transform phase over the full width at half maximum (FWHM) of the associated amplitude peak. The error in this value is estimated as the standard deviation of the Fourier transform phase over the same spatial frequency range. The inverse of this error times 2π is shown as the red circles in Figure 6d and corresponds

to the resolution of our spectrometer in XUV wavelength fraction units. This demonstrates that our interferometer resolution is better than $\frac{\lambda_{XUV}}{100}$ for all harmonic orders investigated.

To estimate the stability of our apparatus and the reproducibility of the experiment, we took 145 interferograms in about 20 min in the same experimental conditions and computed both the phase value and the error on this phase, as previously described. We then consider the mean value and the standard deviation of the phase over all interferograms weighted with the error determined for each of them. The inverse of the standard deviation times 2π is reproduced in Figure 6d as the black "x"-shaped crosses. This result shows that the long-term stability of our apparatus is good enough to enable us to fully benefit from the high resolution of our mode-conversion interferometer. The definitions of the phase and error used later on are these weighted mean values and standard deviations. Note that in general, a higher precision of the interferometer is observed when it is used in a full beam geometry, like with the Aurore laser. The shot-to-shot stability is also better on a 1-kHz system than on a 20-Hz one. In the next section, we report the phase measurements in rotationally- and vibrationally-excited molecules using our interferometer and the previously described procedure.

5. Inversion of the Harmonic Phase at a Threshold

In this section, we illustrate the interest of TSI in HHG and the benefits of our highly stable interferometer by studying the response of near-threshold harmonics to molecular rotations and vibrations. We first consider HHG from rotationally-excited nitrogen molecules. In 2009, Lock *et al.* [30] reported no phase variations inside nitrogen revival using TSI. This result was used to support a failure of the two-center model [31] in the N_2 highest occupied molecular orbital (HOMO) recombination dipole. This result was almost immediately challenged by phase measurements using other techniques, like gas mixing [12], transient grating spectroscopy [13] and RABBIT(Reconstruction of Attosecond Beating by Interference of two–photon Transitions) [2]. However, to our best knowledge, no further attempts to measure the phase variations inside the revival of nitrogen using TSI were reported. In Figure 7, we show phase measurements inside the revival of N_2 for H_9 to H_{17} using our mode-conversion interferometer and a two-pulse alignment stacker [32]. The first striking feature of Figure 7 is that even after only one kick, the first quarter, first half and third quarter revivals (resp. at 2.06, 4.12 and 6.18 ps) are clearly seen in all harmonic orders studied here. The second kick allows one to couple more energy into the rotational wave packet initiated by the first kick, to increase the degree of alignment and therefore the contrast of the revival trace, which corresponds here to a deeper phase modulation. Being able to follow nitrogen revival through the variations of the high harmonics phase reflects the high stability of our experimental arrangement. We expect that being able to measure phase variations inside molecular revival with good enough resolution will greatly help to understand specific issues, like fractional revivals [33,34].
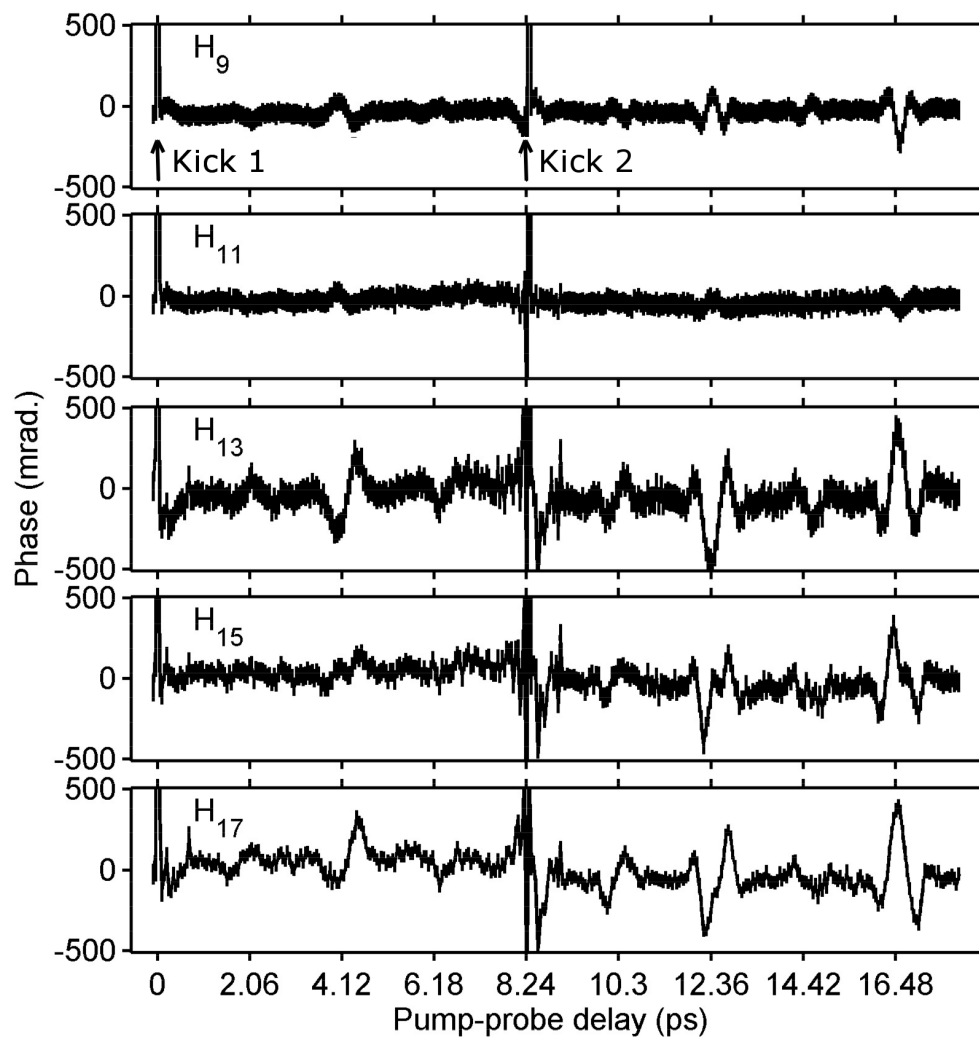
Figure 7. The phase of H_9 to H_{17} generated in nitrogen as a function of the alignment pump-HHG probe delay. Two kickers (indicated with arrows on the first row) separated by one full rotational period (8.24 ps) are used to increase the degree of molecular alignment.

The second piece of information extracted from Figure 7 is that the phase variations change sign when the photon energy crosses the ionization potential (15.58 eV for the HOMO of nitrogen); in our sign convention, the phase of H_9 and H_{11} is maximum at half-revival, whereas it is minimum for H_{13} to H_{17}. Interestingly, H_{11} (which might be below the N_2 effective ionization potential due to the ponderomotive shift [35] in our experimental conditions) is the least contrasted. This could be the result of a destructive interference between two processes contributing to the harmonic emission, like HHG and multiphoton perturbative harmonic generation.

The same kind of inversed behavior in HHG when crossing the ionization threshold was reported in a quantum path-resolved harmonic yield study [36]. For the short trajectories investigated here, this inversion was interpreted as the signature of resonant multiphoton processes. In another kind of experiment, a phase difference between harmonics generated at the threshold in unaligned nitrogen and argon (nitrogen's atomic partner, which is an atomic species with a similar ionization potential) was measured by RABBIT [37,38] and interpreted as the effect on the recombination of the Hopfield

resonance [39] featured by the ionic potential. The full understanding of this inversion, seen both in the phase and the amplitude of the harmonics generated in aligned nitrogen molecules, is beyond the scope of the current paper, but we believe that the phase inversion is important additional information towards this goal. Near the threshold HHG showing particularly interesting features in excited molecules, we investigated another type of excitation: vibrations. We generated harmonics in sulfur hexafluoride [40–43], which has a similar ionization potential to nitrogen and argon.

The results reported by Wagner *et al.* [40] in SF_6 were the very first evidence of time-resolved vibrational quantum beats in molecules followed by HHG self-probing spectroscopy. More recently, phase measurements in vibrationally-excited SF_6 using a transient excitation grating [43] and our mode-conversion interferometer [44] were reported for H_{13} to H_{27}. In Figure 8, we present the results extended to H_9 and H_{11}, that is to harmonic orders below and at a threshold of SF_6 HOMO (15.7 eV), HOMO-1 (16.9 eV), HOMO-2 (17.2 eV) and HOMO-3 (18.3 eV). Our previous studies showed that these orbitals may give non-negligible contributions to the harmonic emission [44]. The four panels of Figure 8 show the oscillations of the phase (first row) and intensity (second row) of H_9 (red) to H_{25} (blue) as a function of the pump-probe delay, filtered at two different vibrational mode frequencies: 774 cm^{-1} (ν_1-A$_{1g}$ mode, first column) and 524 cm^{-1} (ν_2-T$_{2g}$ mode, second column). The first piece of information in Figure 8 is that all harmonic orders show intensity and phase modulations at these two vibrational mode frequencies. Also weaker, the oscillations in the phase signal filtered at 524 cm^{-1} are real and significant. For the three other panels, the oscillations are in phase in all harmonic orders, except one, which shows close to out-of-phase less contrasted oscillations. This is the case for H_{11} (harmonic generated at a threshold of SF_6 HOMO-2) in the phase filtered at 774 cm^{-1}, for H_{13} in the intensity filtered at 774 cm^{-1} and for H_{15} in the intensity filtered at 524 cm^{-1}. As proposed in [44], the dephasing occurring at H_{13} and H_{15} in the oscillations of the intensity could be linked to the shape resonance in the B-channel of SF_6 (corresponding to ionization from and recombination to HOMO-2). The new result presented here is the dephasing in the oscillations of the phase at H_{11}, which we believe is a similar effect to the one observed at the threshold in the revival of nitrogen.

We foresee that all of these experimental results will guide theoretical studies to better understand several issues, such as the mechanism for HHG at the threshold of a molecule, the effect of Hopfield resonances on HHG and also how strong-field ionization populates vibrational levels in different polyatomic molecular cations and how this affects HHG.
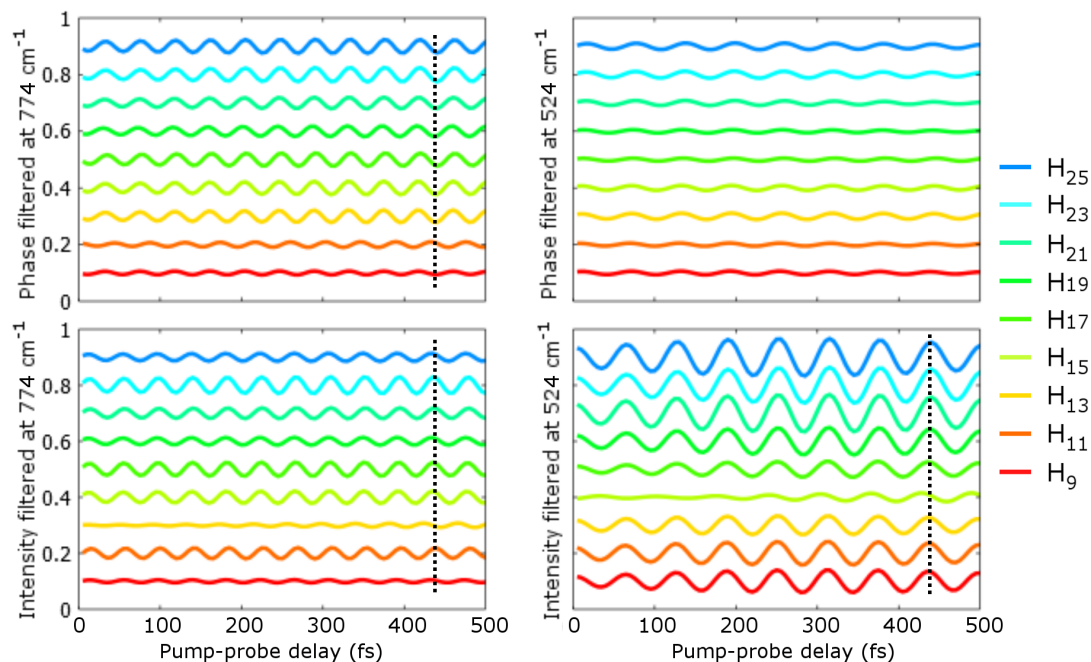
Figure 8. (Color on-line) Phase and intensity of H_9 (red) to H_{25} (blue) generated in SF_6 as a function of the pump-probe delay filtered at two vibrational frequencies (774 and 524 cm^{-1}). All curves are arbitrarily shifted for clarity. The dashed lines help to visualize the relative phase of the oscillations.

6. Conclusions

We reported on a thorough investigation of the spatial mode-conversion TSI arrangement presented in [14]. In particular, we presented overlap integral computations showing that 90.94% of an incident Gaussian beam of waist ω_0 is converted into a TEM_{01} mode of waist $0.58 \times \omega_0$. We emphasized the relation between the IR laser phase-front curvature and the far-field overlap of the two XUV beams when using this mode-conversion device to create two spatially-separated HHG sources at the focus of a lens. We demonstrated the high resolution of this interferometer ($\lambda_{XUV}/100$ down to 27 nm) and the good stability of the overall setup (the standard deviation of the phase measurement is 46.5 mrad at H_{27}).

This arrangement was finally used to investigate the harmonic phase in rotating and vibrating molecules. In particular, we have shown that it is possible to follow N_2 revival and vibrational quantum beats in SF_6 through TSI phase measurements. At the threshold of these two molecules, similar results are observed in the behavior of the phase variations. The harmonic generated at the threshold of the molecule shows an inverted behavior with respect to the harmonic generated above the threshold. More theoretical investigations are needed to determine whether this is an intrinsic or phenomenological feature of HHG in molecules.

Acknowledgments

Author Contributions

Antoine Camper, Yann Mairesse, Nan Lin, Amélie Ferré, Emmanouil Skantzakis, David Staedter and Thierry Ruchon contributed to the experiment in Saclay and Bordeaux. Antoine Camper, Yann Mairesse, Nan Lin, Elizabeth English, Bastian Manschwetus, Pascal Salières and Thierry Ruchon contributed to developing the experimental setup at CEA-Saclay. Dominique Descamps, Frédérique Burgy and Stéphane Petit operated the Aurorelaser at CELIA, and Olivier Gobert operated the LUCA laser at CEA-Saclay. Thierry Auguste and Olivier Gobert performed the IR shaping and mode conversion simulations. Antoine Camper wrote the manuscript, and all authors contributed to its improvement.

Conflicts of Interest

The authors declare no conflicts of interest.

References

1. Zhou, X.; Lock, R.; Li, W.; Wagner, N.; Murnane, M.M.; Kapteyn, H.C. Molecular recollision interferometry in high harmonic generation. *Phys. Rev. Lett.* **2008**, *100*, 073902.
2. Haessler, S.; Caillat, J.; Boutu, W.; Giovanetti-Teixeira, C.; Ruchon, T.; Auguste, T.; Diveki, Z.; Breger, P.; Maquet, A.; Carré, B.; *et al.* Attosecond imaging of molecular electronic wave packets. *Nat. Phys.* **2010**, *6*, 200–206.
3. Smirnova, O.; Mairesse, Y.; Patchkovskii, S.; Dudovich, N.; Villeneuve, D.; Corkum, P.; Ivanov, M.Y. High harmonic interferometry of multi-electron dynamics in molecules. *Nature* **2009**, *460*, 972–977.
4. Schafer, K.J.; Yang, B.; DiMauro, L.F.; Kulander, K.C. Above threshold ionization beyond the high harmonic cutoff. *Phys. Rev. Lett.* **1993**, *70*, 1599.
5. Corkum, P.B. Plasma perspective on strong-field multiphoton ionization. *Phys. Rev. Lett.* **1993**, *71*, 1994.
6. Lewenstein, M.; Balcou, P.; Ivanov, M.; L'Huillier, A.; Corkum, P.B. Theory of high-order harmonic generation by low-frequency laser fields. *Phys. Rev. A* **1994**, *49*, 2117.

7. Maquet, A.; Caillat, J.; Taïeb, R. Attosecond delays in photoionization: Time and quantum mechanics. *J. Phys. B* **2014**, *47*, 204004.

8. Schoun, S.B.; Chirla, R.; Wheeler, J.; Roedig, C.; Agostini, P.; DiMauro, L.F.; Schafer, K.J.; Gaarde, M.B. Attosecond Pulse Shaping around a Cooper Minimum. *Phys. Rev. Lett.* **2014**, *112*, 153001.

9. Mairesse, Y.; Higuet, J.; Dudovich, N.; Shafir, D.; Fabre, B.; Mével, E.; Constant, E.; Patchkovskii, S.; Walters, Z.; Ivanov, M.Y.; *et al.* High Harmonic Spectroscopy of Multichannel Dynamics in Strong-Field Ionization. *Phys. Rev. Lett.* **2010**, *104*, 213601.

10. Paul, P.M.; Toma, E.S.; Breger, P.; Mullot, G.; Augé, F.; Balcou, P.; Muller, H.G.; Agostini, P. Observation of a Train of Attosecond Pulses from High Harmonic Generation. *Science* **2001**, *292*, 1689.

11. Kanai, T.; Takahashi, E.J.; Nabekawa, Y.; Midorikawa, K. Destructive Interference during High Harmonic Generation in Mixed Gases. *Phys. Rev. Lett.* **2007**, *98*, 153904.

12. McFarland, B.K.; Farrell, J.P.; Bucksbaum, P.H.; Gühr, M. High-order harmonic phase in molecular nitrogen. *Phys. Rev. A* **2009**, *80*, 033412.

13. Mairesse, Y.; Dudovich, N.; Zeidler, D.; Spanner, M.; Villeneuve, D.M.; Corkum, P.B. Phase sensitivity of high harmonic transient grating spectroscopy. *J. Phys. B* **2010**, *43*, 065401.

14. Camper, A.; Ruchon, T.; Gauthier, D.; Gobert, O.; Salières, P.; Carré, B.; Auguste, T. High-harmonic phase spectroscopy using a binary diffractive optical element. *Phys. Rev. A* **2014**, *89*, 043843.

15. Kovačev, M.; Fomichev, S.V.; Priori, E.; Mairesse, Y.; Merdji, H.; Monchicourt, P.; Breger, P.; Norin, J.; Persson, A.; L'Huillier, A.; *et al.* Extreme ultraviolet fourier-transform spectroscopy with high order harmonics. *Phys. Rev. Lett.* **2005**, *95*, 223903.

16. Bellini, M.; Lyngå, C.; Tozzi, A.; Gaarde, M.; Hänsch, T.; L'Huillier, A.; Wahlström, C.G. Temporal coherence of ultrashort high-order harmonic pulses. *Phys. Rev. Lett.* **1998**, *81*, 297.

17. Dobosz, S.; Stabile, H.; Tortora, A.; Monot, P.; Reau, F.; Bougeard, M.; Merdji, H.; Carré, B.; Martin, P.; Joyeux, D.; *et al.* Internal frequency conversion extreme ultraviolet interferometer using mutual coherence properties of two high-order-harmonic sources. *Rev Sci Instrum* **2009**, *80*, 113102.

18. Mang, M.M.; Bourassin-Bouchet, C.; Walmsley, I.A. Simultaneous spatial characterization of two independent sources of high harmonic radiation. *Opt. Lett.* **2014**, *39*, 6142–6145.

19. Zerne, R.; Altucci, C.; Bellini, M.; Gaarde, M.B.; Hansch, T.W.; LHuillier, A.; Lynga, C.; Wahlstrom, C.G. Phase-locked high-order harmonic sources. *Phys. Rev. Lett.* **1997**, *79*, 1006–1009.

20. Gariepy, G.; Leach, J.; Kim, K.T.; Hammond, T.J.; Frumker, E.; Boyd, R.W.; Corkum, P.B. Creating High-Harmonic Beams with Controlled Orbital Angular Momentum. *Phys. Rev. Lett.* **2014**, *113*, 153901.

21. Albero, J.; Davis, J.A.; Cottrell, D.M.; Granger, C.E.; McCormick, K.R.; Moreno, I. Generalized diffractive optical elements with asymmetric harmonic response and phase control. *Appl. Opt.* **2013**, *52*, 3637–3644.

22. Ngcobo, S.; Litvin, I.; Burger, L.; Forbes, A. A digital laser for on-demand laser modes. *Nat. Commun.* **2013**, *4*, 2289.

23. Passilly, N.; de Saint Denis, R.; Aït-Ameur, K.; Treussart, F.; Hierle, R.; Roch, J.F. Simple interferometric technique for generation of a radially polarized light beam. *J. Opt. Soc. Am. A* **2005**, *22*, 984–991.

24. Smith, N.L.; Heathcote, W.H.; Hechenblaikner, G.; Nugent, E.; Foot, C.J. Quasi-2D confinement of a BEC in a combined optical and magnetic potential. *J. Phys. B* **2005**, *38*, 223.

25. Meyrath, T.; Schreck, F.; Hanssen, J.; Chuu, C.; Raizen, M. A high frequency optical trap for atoms using Hermite-Gaussian beams. *Opt. Express* **2005**, *13*, 2843–2851.

26. Moll, K.D.; Jones, R.J.; Ye, J. Output coupling methods for cavity-based high-harmonic generation. *Opt. Express* **2006**, *14*, 8189–8197.

27. Salières, P.; L'Huillier, A.; Lewenstein, M. Coherence control of high-order harmonics. *Phys. Rev. Lett.* **1995**, *74*, 3776.

28. Balcou, P.; Salieres, P.; LHuillier, A.; Lewenstein, M. Generalized phase-matching conditions for high harmonics: The role of field-gradient forces. *Phys. Rev. A* **1997**, *55*, 3204–3210.

29. Kumar, M.; Modi, M.H.; Singhal, H.; Chakera, J.A.; Gupta, R.K.; Naik, P.A.; Lodha, G.S.; Gupta, P.D. Measurement of absolute diffraction efficiency of a variable line spaced grating using reflectivity beamline. *AIP Conf. Proc.* **2012**, *1447*, 687–688.

30. Lock, R.M.; Zhou, X.; Li, W.; Murnane, M.M.; Kapteyn, H.C. Measuring the intensity and phase of high-order harmonic emission from aligned molecules. *Chem. Phys.* **2009**, *366*, 22–32.

31. Lein, M.; Hay, N.; Velotta, R.; Marangos, J.P.; Knight, P. Role of the intramolecular phase in high-harmonic generation. *Phys. Rev. Lett.* **2002**, *88*, 183903.

32. Cryan, J.P.; Bucksbaum, P.H.; Coffee, R.N. Field-free alignment in repetitively kicked nitrogen gas. *Phys. Rev. A* **2009**, *80*, 063412.

33. Lock, R.; Ramakrishna, S.; Zhou, X.; Kapteyn, H.; Murnane, M.; Seideman, T. Extracting continuum electron dynamics from high harmonic emission from molecules. *Phys. Rev. Lett.* **2012**, *108*, 133901.

34. Weber, S.J.; Oppermann, M.; Marangos, J.P. Role of Rotational Wave Packets in Strong Field Experiments. *Phys. Rev. Lett.* **2013**, *111*, 263601.

35. Freeman, R.R.; Bucksbaum, P.H. Investigations of above-threshold ionization using subpicosecond laser pulses. *J. Phys. B* **1991**, *24*, 325.

36. Soifer, H.; Botheron, P.; Shafir, D.; Diner, A.; Raz, O.; Bruner, B.; Mairesse, Y.; Pons, B.; Dudovich, N. Near-threshold high-order harmonic spectroscopy with aligned molecules. *Phys. Rev. Lett.* **2010**, *105*, 143904.

37. Wabnitz, H.; Mairesse, Y.; Frasinski, L.J.; Stankiewicz, M.; Boutu, W.; Breger, P.; Johnsson, P.; Merdji, H.; Monchicourt, P.; SaliÃłres, P.; *et al.* Generation of attosecond pulses in molecular nitrogen. *Eur. Phys. J. D* **2006**, *40*, 305–311.

38. Kato, K.; Minemoto, S.; Sakemi, Y.; Sakai, H. Phase differences of near-threshold high-order harmonics generated in atoms and molecules. *Phys. Rev. A* **2014**, *90*, 063403.

39. Haessler, S.; Fabre, B.; Higuet, J.; Caillat, J.; Ruchon, T.; Breger, P.; Carré, B.; Constant, E.; Maquet, A.; Mevel, E.; *et al*.   Phase-resolved attosecond near-threshold photoionization of molecular nitrogen. *Phys. Rev. A* **2009**, *80*, 011404.

40. Wagner, N.L.; Wüest, A.; Christov, I.P.; Popmintchev, T.; Zhou, X.; Murnane, M.M.; Kapteyn, H.C.   Monitoring molecular dynamics using coherent electrons from high harmonic generation. *Proc. Natl. Acad. Sci. USA* **2006**, *103*, 13279–13285.

41. Walters, Z.B.; Tonzani, S.; Greene, C.H. High harmonic generation in SF 6 : Raman-excited vibrational quantum beats. *J. Phys. B* **2007**, *40*, F277.

42. Walters, Z.B.; Tonzani, S.; Greene, C.H. Vibrational interference of Raman and high harmonic generation pathways. *Chem. Phys.* **2009**, *366*, 103–114.

43. Ferré, A.; Staedter, D.; Burgy, F.; Dagan, M.; Descamps, D.; Dudovich, N.; Petit, S.; Soifer, H.; Blanchet, V.; Mairesse, Y.; *et al*.   High-order harmonic transient grating spectroscopy of SF6 molecular vibrations. *J. Phys. B* **2014**.

44. Ferré, A.; Boguslavskiy, A.; Dagan, M.; Blanchet, V.; Bruner, B.; Burgy, F.; Camper, A.; Descamps, D.; Fabre, B.; Fedorov, N.; *et al*. Multi-channel Electronic and Vibrational Dynamics in Polyatomic High-order Harmonic Generation. *Nat. Commun.* **2014**, *6*, 5952.